Apoptosis 2005; **10**: 1317–1331

DOI: 10.1007/s10495-005-2718-x

Biphasic behavior of changes in elemental composition during staurosporine-induced apoptosis

F. Arrebola, J. Cañizares, M. A. Cubero, P. V. Crespo, A. Warley and E. Fernández-Segura

Department of Histology, Faculty of Medicine, University of Granada, E-18071 Granada, Spain (F. Arrebola, J. Cañizares, M. A. Cubero, P. V. Crespo, E. Fernández-Segura); Institute of Neurosciences, University of Granada, E-18071 Granada, Spain (J. Cañizares, P. V. Crespo, E. Fernández-Segura); CUI King's College London, Guy's Campus, London, SE1 1UL, UK (A. Warley)

Published online: 3 October 2005

Although the identification of events that occur during apoptosis is a fundamental goal of apoptotic cell death research, little is know about the precise sequence of changes in total elemental composition during apoptosis. We evaluated total elemental composition (Na, Mg, P, Cl, S, and K) in relation to molecular and morphological features in human U937 cells induced to undergo apoptosis with staurosporine, an intrinsic pathway activator. To evaluate total elemental content we used electron probe X-ray microanalysis to measure simultaneously all elements from single, individual cells. We observed two phases in the changes in elemental composition (mainly Na, Cl and K). The early phase was characterized by a decrease in intracellular K ($P < 0.001$) and Cl ($P < 0.001$) content concomitant with cell shrinkage, and preceded the increase in proteolytic activity associated with the activation of caspase-3. The later phase started with caspase-3 activation, and was characterized by a decrease in the K/Na ratio ($P < 0.001$) as a consequence of a significant decrease in K and increase in Na content. The inversion of intracellular K and Na content was related with the inhibition of Na^+/K^+ ATPase. This later phase was also characterized by a significant increase ($P < 0.001$) in intracellular Cl with respect to the early phase. In addition, we found a decrease in S content and an increase in the P/S ratio. These distinctive changes coincided with chromatin condensation and DNA fragmentation. Together, these findings support the concept that changes in total elemental composition take place in two phases related with molecular and morphological features during staurosporine-induced apoptosis.

Keywords: apoptosis; apoptotic volume decrease; caspases; chlorine; electron probe X-ray microanalysis; Na^+/K^+ ATPase; PARP; potassium; sodium.

Introduction

Apoptosis is a form of cell death defined by biochemical and morphological changes including a decrease in cell volume, caspase activation, chromatin condensation, DNA laddering and cell fragmentation. A hallmark of apoptosis in a variety of cell types is the loss of cell volume or cell shrinkage, termed apoptotic volume decrease (AVD).[1] Different studies demonstrated that cell shrinkage was associated with a loss of intracellular monovalent ions, fundamentally K^+,[2–5] and with an early increase in outward K^+ currents through voltage-gated K^+ (K_v),[6–9] Ca^{2+}-activated K^+ (K_{Ca}),[10,11] or 2-pore K^+ (K2P) channels.[12] It has been well documented that maintenance of normal physiological intracellular K^+ concentrations by attenuating potassium efflux with pharmacological blockage of K^+ channels[8,13] or by increasing extracellular K^+,[2,14] decelerates apoptotic cell shrinkage and attenuates apoptosis in different cell lines. It was recently shown that overexpression of the human *KCNA5* gene, which encodes a delayed-rectifier voltage-gated K^+ channel, increases K^+ currents, accelerates AVD, and induces apoptosis in rat pulmonary artery smooth muscle cells.[15]

In spite of the abundance of data that implicate K^+ in cell shrinkage, less is understood about the accompanying changes in other monovalent ions such as Cl^- and Na^+ during apoptosis.[9,16,17] Interestingly, the demonstration that induction of AVD under normotonic conditions is coupled to regulated volume decrease (RVD) facilitation suggests the participation of Cl^- in promoting apoptotic events that lead to cell death.[1,13] The activation of the outwardly rectifying chloride channel in CD95-induced cell death in T lymphocytes[16] and the tumor necrosis factor-α in HTC hepatoma cells[9] support this possibility. Also, a recent study showed that Na^+ influx is required for volume loss during anti-Fas-induce apoptosis.[18]

In addition to cell shrinkage, caspase activation is a fundamental feature of apoptosis. Two classes of caspase have been identified: (1) initiator caspases such as caspase-8 and -9, which tend to have a longer pro-domain and bind to adaptor molecules, and (2) effector caspases with short pro-domains such as caspase-3, -6 and -7, which are activated by the action of upstream initiator caspases

Correspondence to: E. Fernández-Segura, Department of Histology, Faculty of Medicine, University of Granada, E-18071 Granada, Spain. Tel.: +34 958-243515; Fax: +34 958-244034; e-mail: efsegura@ugr.es

and are involved in the execution phase of apoptosis.[19,20] Accumulated evidence now suggests that changes in intracellular ion homeostasis, mainly K^+, appear to be required for activation of the molecular machinery during apoptosis, including initiator and effector caspases. The efflux of K^+ ions has been related to cytochrome *c*-dependent formation of the apoptosome[21] and activation of caspase-3 like enzymes.[2,14] In addition, K^+ efflux has been implicated in the activation of apoptotic nuclease, DNA degradation[3] and ribosomal RNA degradation.[22]

Emerging evidence suggests that Cl^- and Na^+ fluxes may play important roles in key events in the execution of apoptosis. Caspase-3 activation and DNA laddering were blocked by a Cl^- channel blocker in different cell types exposed to death receptor- or mitochondrion-inducers of apoptosis.[13] Also, Cl^- efflux has been related with the activity of DNA fragmentation factor 40 (DFF40), responsible for chromatin condensation and oligonucleosomal fragmentation of DNA.[23] It was recently reported that sodium (Na^+) is involved in early phosphatidylserine exposure in thymocyte apoptosis induced by extracellular ATP.[24]

Taken together, these studies suggested that fluxes of intracellular ions such as K^+, Cl^- and Na^+ across the plasma membrane are involved in the progression of apoptosis. However, a number of important issues remain unclear. No information is available on the precise sequence of changes in total ion composition, and the exact relationship between changes in cation and anion concentrations at the single cell level during apoptosis has yet to be documented. In addition, little is known about the relationship between changes in total ion homeostasis and morphological and biochemical events of apoptosis such cell shrinkage, caspase activation, chromatin condensation and DNA fragmentation. The lack of studies on these phenomena is probably a result of methodological problems with the accurate measurement of total intracellular ion composition in single, individual cells with fluorescent ion-indicator dyes.

To address the above issues, we used electron probe X-ray microanalysis (EPXMA), which is an electron microscopy (EM) technique that allows multiple elements (Na, Mg, P, Cl, S, K) to be measured simultaneously in single, individual cells. Also, EPXMA is a viable alternative and complementary technique to fluorescent ion-binding dyes.[25] Although EPXMA has been used previously to characterize elemental composition under different experimental conditions, it has rarely been used to characterize elemental alterations during apoptosis. In addition, a detailed time-course of changes in elemental composition during apoptosis and their relation with morphological and early molecular features has not been reported. Here we used EPXMA to examine the temporal relationship between changes in total elemental (Na, Mg, P, Cl, S, K) composition and morphological and biochemical events that characterize the apoptotic process (*i.e.*, changes in cell volume, caspase-3 activation, chromatin condensation and nuclear DNA fragmentation) in human monoblastic U937 cells during staurosporine (STS)-mediated apoptosis.

Material and methods

Cell culture and treatment

U937 cells were obtained from the European Collection of Cell Cultures (ECACC, Wiltshire, UK) and cultured in RPMI 1640 medium supplemented with 10% heat-inactivated bovine fetal serum and 2 mM L-glutamine (all from Sigma-Química, Madrid, Spain). Cells were maintained at 37°C in a humidified atmosphere containing 5% CO_2. To induce apoptosis, U937 cells grown (5×10^5 cell/ml) in complete RPMI 1640 medium without phenol red were treated with 1 μM STS (Sigma-Química, Madrid, Spain) at 37°C.

Assessment of apoptosis

Cell apoptosis was evaluated by nuclear staining with Hoechst 33342 (Sigma-Química, Madrid, Spain) and DNA fragmentation. For Hoescht 33342 staining, cells were collected, fixed with 4% formaldehyde, and stained with Hoechst 33342 (5 μg/ml). Cells were examined with a Leitz Laborlux 12 microscope (Leica, Barcelona, Spain) equipped for epi-fluorescence illumination. Nuclear morphology was evaluated with an excitation wavelength of 355–425 nm and a longpass filter of 470 for emission. Fluorescence images were acquired with a Leica DC100 digital camera (Leica, Barcelona, Spain) and were processed with Adobe PhotoDeluxe software (Adobe System, San Jose, CA).

To determine internucleosomal DNA cleavage, cells were washed twice with ice-cold PBS buffer and digested with lysis buffer (20 mM Tris-HCl, pH 7.5, 2 mM EDTA, 0.4% Triton X-100) for 15 min at 4°C. Cell lysates were centrifuged at 13 000×*g* for 15 min and incubated with proteinase K (100 μg/ml) and RNase A (60 μg/ml) for 3 h at 55°C. The DNA was extracted with an equal volume of phenol/chloroform/isoamyl alcohol (25:24:1). DNA samples were analyzed by electrophoresis on 1.2% agarose gels, followed by staining with ethidium bromide.

Assessment of cell viability

Cell viability was assessed in 96-well plates by measuring lactate dehydrogenase (LDH) released into the culture medium with a colorimetric assay (Roche Diagnostics,

Barcelona, Spain) according to the manufacturer's instructions. Absorbance was determined at 490 nm in an ELX 800 universal microplate reader (Bio-Tek Instruments Inc, Winosski, VT).

Caspase-3 activity assay

N-acetyl-Asp-Glu-Val-Asp-p-nitro-aniline (DEVD-pNA) cleavage activity from cytosolic extract was measured using a colorimetric assay (R&D Systems, Minneapolis, MN). In brief, U937 cells were collected at different time intervals by centrifugation at $400\times g$ for 5 min at 4°C, and were resuspended in chilled lysis buffer. After 10 min on ice the supernatant was collected by centrifugation, assayed for protein content with the BCA protein assay (Pierce Biotechnology, Rockford, IL), and incubated at 37°C in reaction buffer containing DEVD-pNA substrate for caspase activity measurements. After 1 h of incubation, release of the chromogenic compound pNA was measured by absorbance at 405 nm using an ELX 800 universal microplate reader (Bio-Tek Instruments Inc., Winooski, VT).

Immunocytochemistry

Expression of cleaved caspase-3 and poly(ADP)-ribose polymerase (PARP) were assayed by immunocytochemistry. To detect active caspase-3, the cleaved caspase-3 antibody was used to detect endogenous levels of the large fragment (17/19 kDa) of activated caspase-3 resulting from cleavage adjacent to Asp 175 (Cell Signaling Technology, Beverly, MA). Cleavage of PARP was detected with the human specific cleaved PARP (214) antibody, which detects endogenous levels of the large fragment (89 kDa) of human PARP (Cell Signaling Technology, Beverly, MA). Immunocytochemical assays were done with the MLINK streptavidin-biotin-immunoperoxidase kit (Master Diagnostics, Granada, Spain). Briefly, cells were washed with PBS, dropped onto poly-L-lysine coated slides and fixed with 10% buffered formaldehyde. Samples were then permeabilized with 0.2% Triton X-100 in PBS, and were incubated with blocking buffer and then incubated with the primary antibody diluted at 1:100 in blocking buffer during overnight at 4°C. After this the cells were incubated with biotinylated anti-rabbit IgG secondary antibody for 30 min, washed with PBS, and incubated with streptavidin-biotin-peroxidase complex. The peroxidase reaction was visualized with 0.05% diaminobenzidine and 0.01% hydrogen peroxide. Images were acquired with a Leica DC100 digital camera (Leica, Barcelona, Spain) and were processed with Adobe PhotoDeluxe software (Adobe System, San Jose, CA).

Cell volume measurements

Changes in cell volume were estimated from cellular diameter (d). Cell volume (V) is related to d by the equation $V = 4/3\pi r^3$, assuming that the cell swells and shrinks in a spherical manner.[26] Cell diameter was measured with the scale bar of the Philips XL30 scanning electron microscope (Philips, Eindhoven, Netherlands) before the cellular X-ray spectra were obtained with EPXMA. Data were normalized to control values and expressed as relative cell volume changes.

X-ray microanalysis

Cells were prepared for X-ray microanalysis as previously described.[27] Briefly, cells were removed from the culture medium and transferred into polycarbonate tissue culture plate well inserts (Millipore, Bedford, MA), which were in turn transferred to conical centrifuge tubes and centrifuged at $170\times g$ for 3–5 min. After centrifugation, polycarbonate membrane filters were cut from their polystyrene holder and washed with ice-cold distilled water for 5 s to remove the culture medium. This procedure does not significantly alter the elemental composition of different cell lines. The samples were washed and plunge-frozen in liquid nitrogen (LN_2), and placed in a precooled aluminum specimen holder at LN_2 temperature. The specimen holder was then transferred to an Emitech K755 freeze-drier (Emitech, Ashford, UK), and cells were freeze-dried in three 1-h steps at −100°C, −70°C and −50°C separated by a 1-h interval during which the temperature was raised.[28] The membrane filters were then fixed to adhesive graphite lamina on stubs, and coated with carbon in a high-vacuum coating system (Emitech, Ashford, UK).

X-ray microanalysis was performed on whole freeze-dried U937 cells in a Philips XL30 scanning electron microscope (Philips, Eindhoven, Netherlands). The microscope was equipped with an UTW Si(Li) energy-dispersive X-ray detector (EDAX International, Tilburg, Netherlands). The analytical conditions were: tilt angle 35°, take-off-angle 61.34° and working distance 10 mm. X-ray spectra were acquired at an accelerating voltage of 10 kV and collected in the static spot mode for 200 s live time. Only one spectrum was acquired from each cell. The concentration of elements in the specimen was obtained with the peak-to-local-background (P/B) ratio method.[29] Cell element concentrations were obtained with reference to 20% dextran standards containing known amounts of inorganic salts.[30]

When element concentrations were determined by EPXMA, symbols for each element are given without the oxidative state, *i.e.*, Na. However, for data referred to as free ion concentration, the oxidative state is given, *i.e.*, Na^+.

Rubidium uptake assay

For rubidium (Rb) uptake determinations with X-ray microanalysis, 5 mM RbCl was added to U937 cells (5×10^5 cell/ml) cultured in complete medium in the presence or absence of 1 μM STS. All samples were incubated at 37°C in a 5% CO_2 atmosphere. At the indicated time, cells were processed for X-ray microanalysis as indicated above. Intracellular Rb content was used as an indicator of Rb uptake. For Rb content, semiquantitative data for Rb Lα peaks were obtained with the P/B ratio method.

Na^+/K^+-ATPase activity assay

The functional expression of the Na^+/K^+-ATPase was assessed as the ouabain-sensitive uptake of Rb, as described previously.[31] We adapted the routine isotope ($^{86}Rb^+$) uptake method for EPXMA. In brief, 15 min prior to assay, cells (5×10^5 cell/ml) cultured in complete RPMI 1640 medium in the presence or absence of 1 μM STS were treated with 1 mM ouabain for the fraction of cells used for ouabain-insensitive transport. Rubidium uptake was started by adding 5 mM RbCl to the fraction of cells used for total and ouabain-insensitive Rb uptake from control and STS-treated cells, and the mixture was incubated at 37°C in a 5% CO_2 atmosphere for 10 min. The cells were then cryoprocessed for X-ray microanalysis as described above. Transport activity was expressed as Rb content, used as indicator of Rb uptake, and the difference between Rb content in the presence and absence of ouabain was taken as ouabain-sensitive Rb uptake (net activity). For Rb content, semiquantitative data for Rb Lα peaks were obtained with the P/B ratio method.

Statistical analysis

Data were expressed as the mean ± standard error of mean. Multiple experimental groups were compared using one-way ANOVA followed by Newman-Keuls test or the Kruskal-Wallis test followed by Dunn's test for multiple pairwise comparisons. To compare two experimental groups, we used the Mann-Whitney test. P values less than 0.05 were considered statistically significant. All statistical analyses were done with the GraphPad InStat 3.00 program for Windows (GraphPad Software, San Diego, CA).

Results

STS-induced apoptosis

We first analyzed the induction of apoptosis in U937 cells after treatment with 1 μM STS, a mitochondrion-mediated apoptosis inducer. Apoptosis was assessed by evaluating two typical features: chromatin condensation and oligonucleosomal DNA fragmentation. Figure 1A illustrates the time-course of changes in the chromatin pattern with Hoechst 33342 staining. The percentages of cells with condensed or fragmented chromatin are shown in Figure 1B. After 2 h of STS exposure, the changes in chromatin started to become evident. Between 3 and 5 h, most U937 cells showed apoptotic features. This time-dependent response consisting of changes in chromatin was accompanied by a time-dependent fragmentation of oligonucleosomal DNA as evaluated by conventional gel electrophoresis (Figure 1C). DNA laddering was evident from 3 h after incubation with STS. These morphological and biochemical events not were associated with the loss of plasma membrane integrity as evaluated by the release of LDH to the extracellular medium (Figure 1B).

STS-induced caspase-3 activation

Proteolytic activity associated with caspase-3 was measured as the capacity of the cytosolic extract to cleave the colorimetric peptide substrate DEVD-pNA, and as the reactivity of antibodies that recognize the cleaved form of caspase-3 and PARP (Figure 2). The exposure of U937 cells to STS caused a time-dependent DEVD-pNA cleavage, which started to increase after 1 h of exposure to the drug, and reached statistical significance ($P < 0.05$) after 2 h compared to control cells. Before 2 h, no significant differences were seen. After 3 h, no further increase in DEVD-pNA cleavage activity could be detected (Figure 2A). Next, we examined the immunocytochemical staining for cleaved caspase-3, visible as dark-brown punctate deposits, and detectable with a polyclonal antiserum that recognizes the large fragment (17/19 kDa) resulting from cleavage at the Asp 175 residue (Figure 2B). Quantitative determinations showed that STS-induced a time-dependent increase in the active form of the enzyme (Figure 2C). Cleavage of caspase-3 first became significant ($P < 0.001$) from 2 h after treatment with STS, and showed a time-dependent sequence of changes parallel to those seen for caspase-3 activity with the DEVD-pNA substrate. Figure 2D shows the immuno-cytochemical pattern for PARP obtained with a polyclonal antibody that detects only the cleaved form. As with DEVD-pNA activity and active caspase-3 reactivity, the PARP cleaved product became detectable ($P < 0.001$) from 2 h after treatment with STS (Figure 2E).

Cell volume during STS-induced apoptosis

A hallmark of apoptosis is the normotonic reduction in cell volume. To investigate this in STS-induced apoptosis

Figure 1. Time-course of changes in nuclear morphology, LDH release and DNA fragmentation in staurosporine-treated U937 cells. *A,* Fluorescence micrographs of nuclear morphology in untreated and 1 μM STS-treated U937 cells. Nuclear morphology was evaluated in fixed cells after staining with 5 μM Hoechst 33342 dye for 30 min. *B,* Percentage of condensed nuclei in U937 cells stained with Hoechst 33342 (*closed circles*) and LDH release (*open circles*) after drug exposure. Note that the number of cells with condensed chromatin increased significantly after 2 h of exposure to the drug. The time-course response in nuclear chromatin was not accompanied by the release of LDH to the extracellular medium. Data are given as the mean ± SE of seven independent experiments. *C,* DNA fragmentation induced by STS as determine by agarose gel electrophoresis. DNA laddering was seen from 3 h of drug exposure. The image is representative of four independent experiments.

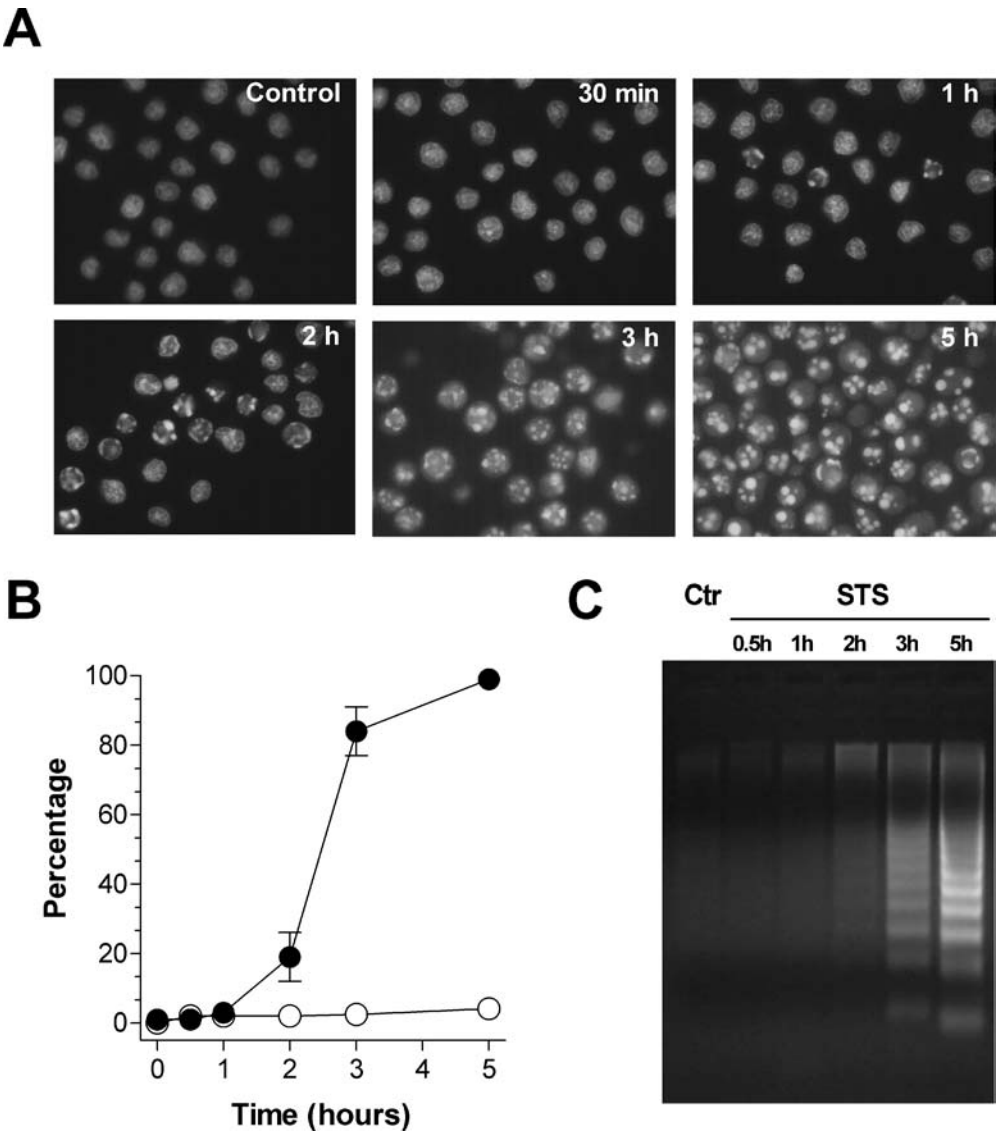

in U937 cells, we evaluated the temporal changes in volume by measuring alterations in cell diameter, assuming that U937 cells shrink or swell in a spherical form. To support this assumption, we examined changes in cell shape of whole, freeze-dried U937 cells. Figure 3A shows scanning electron micrographs of untreated and STS-treated cells, showing that apoptosis induced by STS is not accompanied by extensive irregular changes in cell shape such as membrane blebbing. The lack of membrane blebs has been previously documented in STS-treated human promyelocytic leukemia (HL-60), Burkitt lymphoma (CA46), and mouse (PC-12) cells.[32,33] Figure 3B shows that exposure to STS induced a significant ($P < 0.01$) decrease in cell volume, which became evident after 30 min of drug exposure. After 30 min the cells continued to shrink during exposure to STS, with nonsignificant variations that did not reach statistical significance. After 5 h, cell volume was markedly decreased ($P < 0.001$) in comparison with previous time points.

Figure 2. Time-course of proteolytic activity associated with caspase-3 in staurosporine-treated U937 cells. *A*, Activation of DEVD-specific caspase was measured with the colorimetric substrate DEVD-pNA. *B*, Immunocytochemical staining of caspase-3 cleavage with the human cleaved caspase-3 (Asp175) antibody. Dark brown punctuate deposits represent the 17/19-kDa active form of caspase-3. *C*, Quantitative determination of caspase-3 cleavage. *D*, Immunocytochemical staining of PARP cleavage with the human cleaved PARP (Asp214) antibody. Dark brown punctuate deposits represent the 89-kDa cleaved form of PARP. *E*, Quantitative determination of PARP cleavage. Note that DEVD-pNA cleavage activity, as well as caspase-3 and PARP cleavage, became significant after 2 h after treatment with STS. Data are given as the mean ± S.E. of three independent experiments. Values with different superscripts (a and b) are significantly different from each other according to analysis of variance and Student-Newman-Keuls multiple comparisons test.

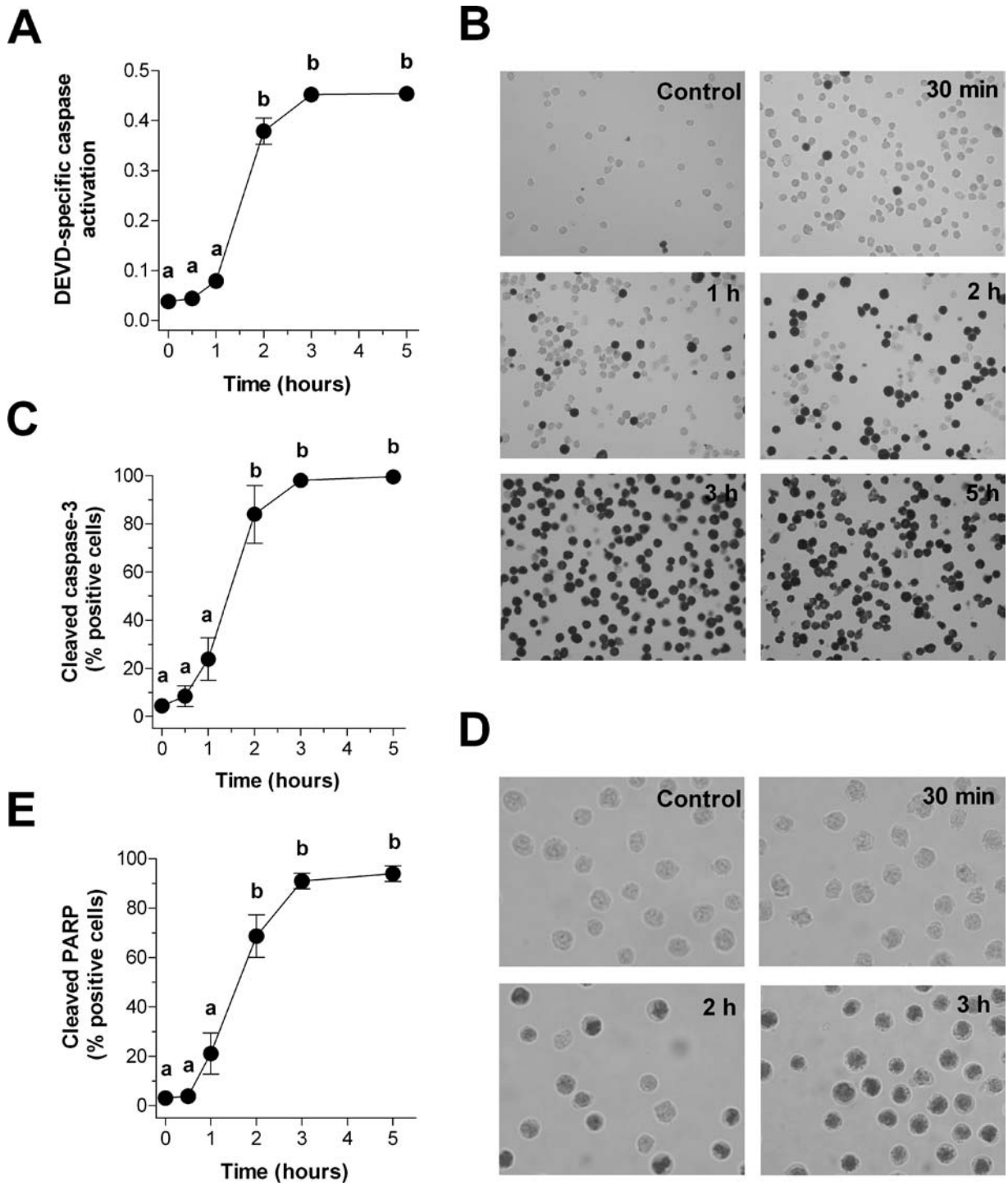

Figure 3. Time-course of changes in cell shape (A) and volume (B) in staurosporine-treated U937 cells. *A.* Scanning electron micrographs of whole, freeze-dried cells before and after treatment with 1 μM staurosporine. At different times, U937 cells were centrifuged into polycarbonate tissue culture inserts, washed with distilled water, plunge-frozen in liquid nitrogen, freeze-dried and evaporated with carbon (Scale bar: 10 μm). *B.* Cell volume was estimated from cellular diameter with the equation $V = 4/3\pi r^3$, assuming that U937 cells shrink in a spherical manner. Cell diameter was measured with the scale bar of the Philips XL30 scanning electron microscope before the cellular X-ray spectra were obtained from whole, freeze-dried cells. Data were normalized to control values and expressed as relative cell volume changes. Note that the loss of cell volume occurs in two phases: an early phase to 30 min, and a later phase after 5 h of drug exposure. Data are given as the mean ± S.E. of three independent experiments. For each column, data with different superscripts (a, b, and c) are significantly different from each other according to analysis of variance and Student-Newman-Keuls multiple comparisons test.

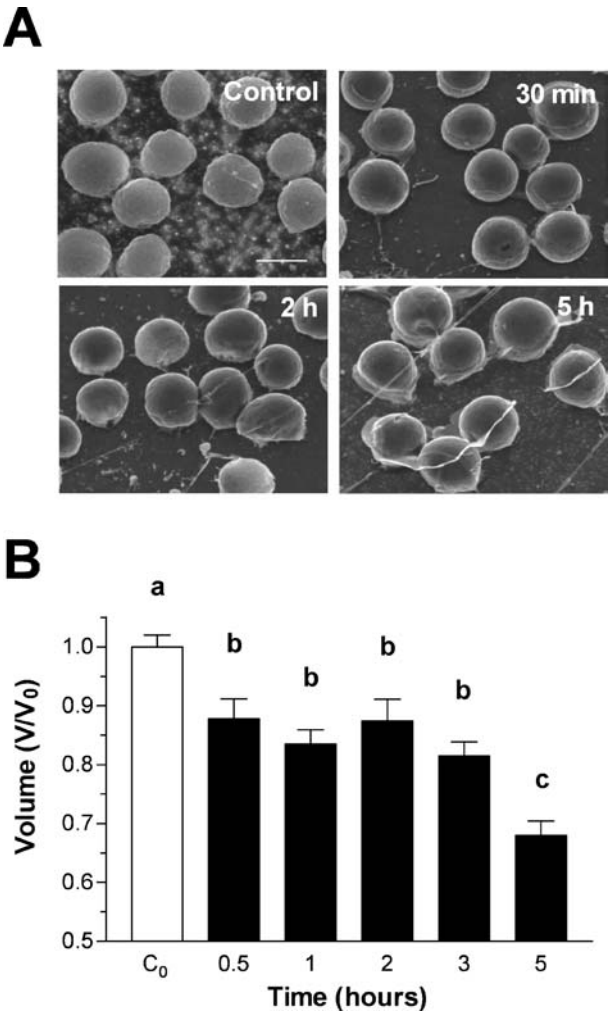

STS-induced electrolyte changes

To examine the temporal relationship between the loss of cell volume, proteolytic activity associated with caspase-3, changes in chromatin features, and DNA fragmentation with alterations in total elemental content, we performed both qualitative and quantitative analysis at the whole cell level by X-ray microanalysis with scanning EM. Figure 4A shows X-ray spectra from control and STS-treated U937 cells. In untreated control cells the elemental profile was characterized by high peaks of K and P, low Na peak, and intermediate peak of Cl. This analytical profile in untreated control U937 cells was similar to that obtained with X-ray microanalysis in different experimental cell models. In STS-treated cells, X-ray spectra show time-dependent variations in the peaks for Na, S, Cl, and K. However, the peaks for P and Mg were almost identical in all spectra.

Figure 4B shows the time-dependent changes in intracellular concentrations (mmol/kg dry weight) of Na, Mg, P, Cl, S and K from human U937 cells treated with STS. After 30 min, elemental analysis showed a selective and significant ($P < 0.001$) loss of Cl and K content. No significant differences were found for Na, Mg, P or S. There were no differences in P content between control and STS-treated cells, and the content of this element remained stable throughout the 5 h of treatment. After 1 h the decreases in K and Cl were steady and significant ($P < 0.001$) compared to control cells. After 2 h elemental analysis showed a further reduction in K and an increase in Na ($P < 0.001$) with respect to earlier time points. After this time intracellular Cl content began to increase, although its concentration remained significantly lower than in control cells.

After 3 h STS-treated cells showed a significant increase in Na ($P < 0.001$). There were no differences in K concentration between 2 and 3 h. At this time the S content began to decrease significantly ($P < 0.001$). After 5 h, K was markedly decreased ($P < 0.001$) in comparison to earlier time points. Sodium concentrations also increased, and Cl continued to increase in comparison to the content recorded after 1 h.

A major problem with EPXMA of cells cultured onto a thick substrate and analyzed with scanning EM is overpenetration of the electron probe in the sample, which can lead to lower P/B ratios. To obviate this problem, elemental concentrations were normalized to the P content as a measure of the cellular mass under the beam. This criterion was validated by the absence of differences in mean *P* content between control and treated cells, and by the close linear relationship between intracellular *K* and *P*.[34] Figure 5 summarizes the data for Na/P, Cl/P and K/P content ratios in U937 cells treated with 1 μM STS during 5 h. The time-course of changes in elemental ratios were similar to the pattern seen for absolute concentrations. These data also suggested that under our analytical conditions, the effect of possible technical artifacts was negligible.

Figure 6 shows the findings for P/S ratio, which increased significantly ($P < 0.001$) after 3 h of treatment

Figure 4. Time-course of total elemental composition in staurosporine-treated U937 cells. Untreated and STS-treated cells were processed as explained in the legend to Figure 3. *A*, Representative X-ray spectra derived from whole single, individual cells at each period after exposure to STS. Spectra were acquired at 10 kV and were collected in the static spot mode for 200 s live time. *B*, Intracellular elemental concentration (mmol/kg dry weight) of sodium, chlorine, potassium, phosphorous, magnesium, and sulfur. Cell element concentrations were obtained with reference to 20% dextran standards containing known amounts of inorganic salts. Data are given as the mean ± S.E. of five independent experiments (15 measurements per experiment). For each column, data with different superscripts (a, b, c, and d) are significantly different from each other according to the Kruskall-Wallis test and Dunn's multiple comparisons test.

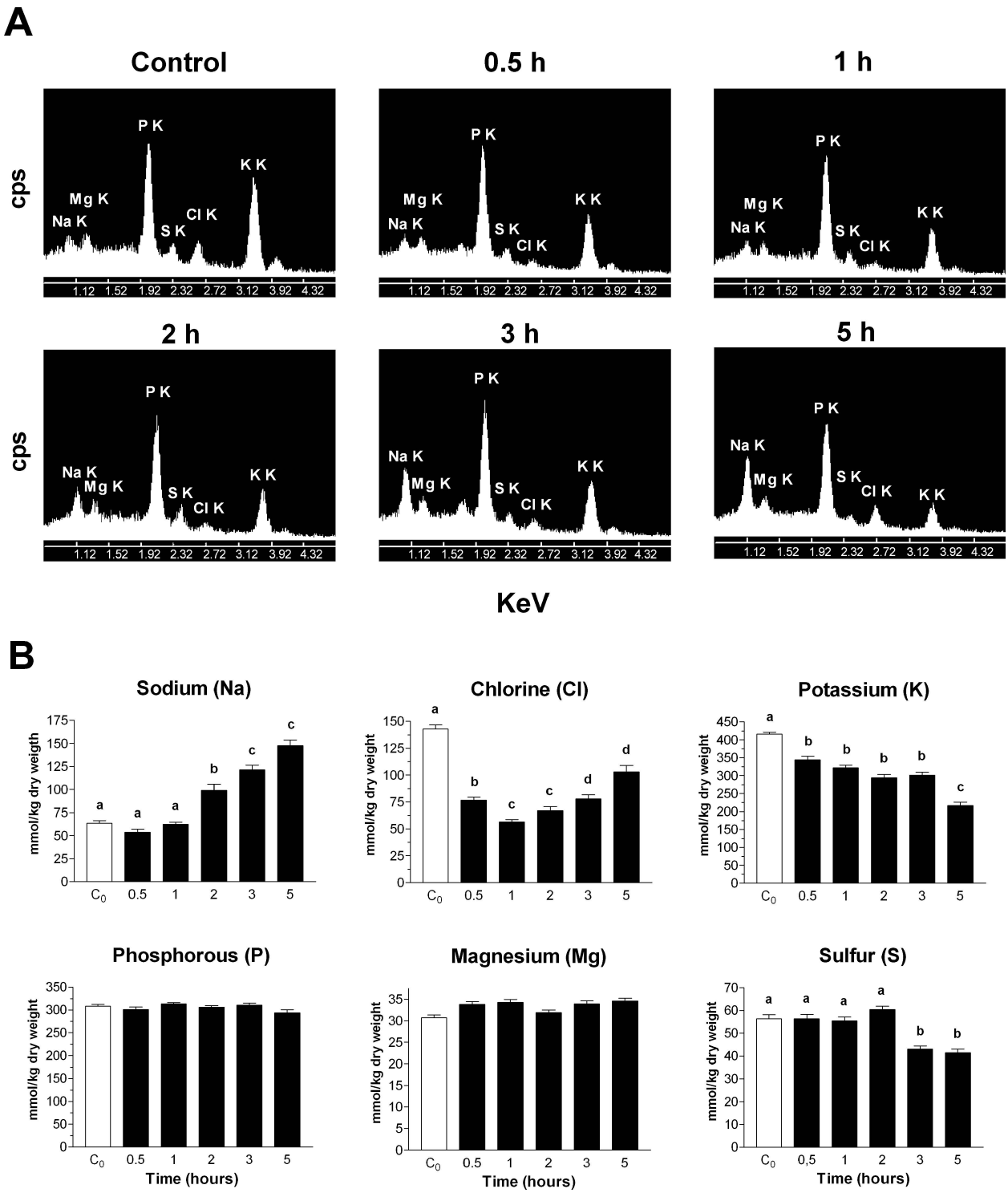

Figure 5. Time-course of Na/P, Cl/P and K/P ratios in staurosporine-treated U937 cells. Untreated and STS-treated cells were processed as explained in the legend to Figure 4. Note that the time-course of elemental ratios was similar to the time-course for absolute concentrations. Data are given as the mean ± S.E. of five independent experiments (15 measurements per experiment). For each column, data with different superscripts (a, b, c, and d) are significantly different from each other according to the Kruskall-Wallis test and Dunn's multiple comparisons test.

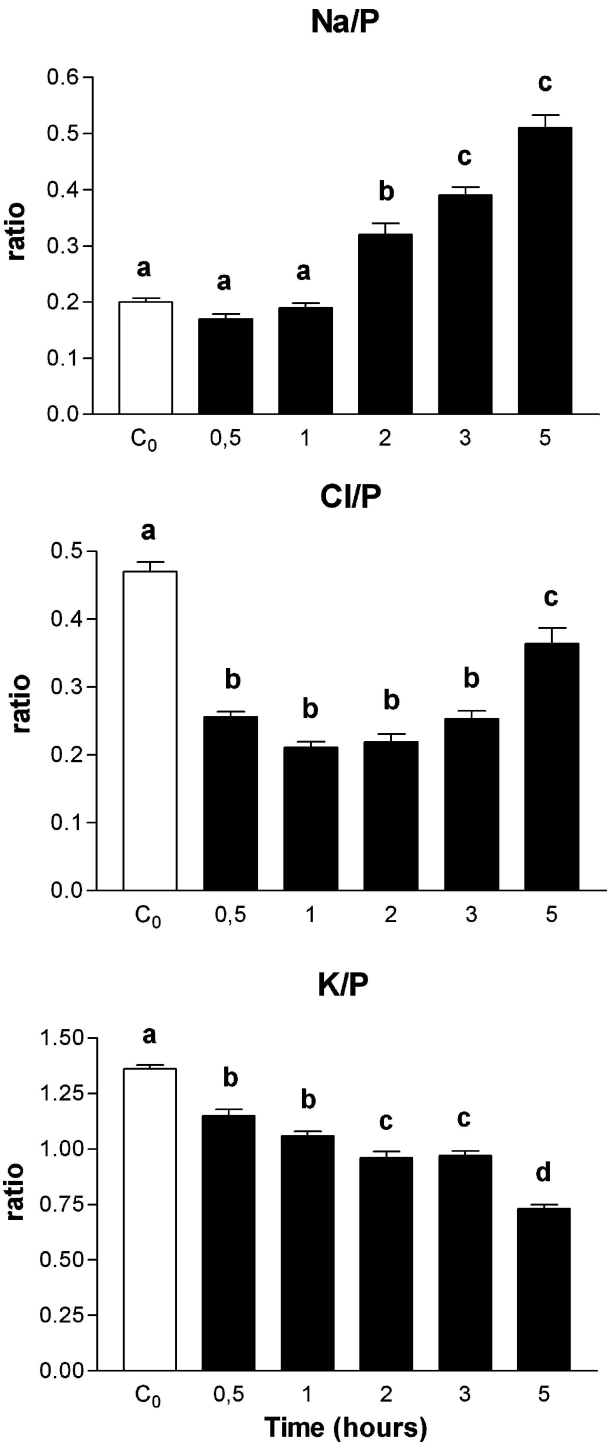

Figure 6. Time-course of P/S and K/Na ratios in staurosporine-treated U937 cells. Untreated and STS-treated cells were processed as indicated in Figure 4. Data are given as the mean ± S.E. of five independent experiments (15 measurements per experiment). For each column, data with different superscripts (a, b, c, and d) are significantly different from each other according to the Kruskall-Wallis test and Dunn's multiple comparisons test.

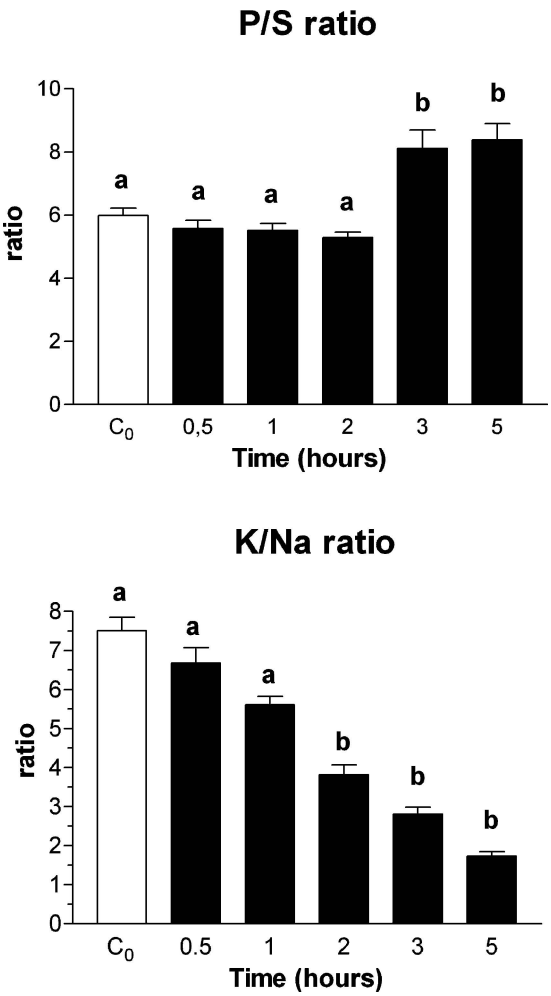

as a result of the decrease in S concentrations. The increase in P/S ratio has been related to the relative increase in the nuclear-to-cytoplasmic ratio that occurs during the late phase of apoptosis. We also calculated the changes in K/Na ratio (Figure 6B), which is a sensitive and quantitatively reliable indicator of cell injury in microanalytical studies.[35] Staurosporine induced a time-dependent decrease in K/Na ratio, which became statistically significant ($P < 0.01$) from 2 h of drug exposure. The significant decrease coincided with caspase-3 activation, PARP cleavage, chromatin condensation and DNA fragmentation.

Functional activity of the Na^+/K^+ ATPase pump during STS-induced apoptosis

The significant decrease in K/Na ratio as a result of the decrease in K and the increase in Na suggested inhibition of the Na^+/K^+ ATPase pump. To investigate this we first examined the transport of K^+ across the plasma membrane during apoptosis induced by STS, using the uptake of the K^+ tracer Rb. Transport activity was expressed as intracellular Rb content, used as an indicator of Rb uptake, and evaluated by EPXMA. Figure 7 shows the time-course of changes in Rb uptake during STS treatment. We found a significant decrease ($P < 0.001$) in Rb uptake after 2 h in comparison with untreated control cells. This decrease coincided with a significant activation of caspase-3 and an increase in intracellular Na and Cl. We then decided to examine the functional expression of the Na^+/K^+ ATPase during STS-induced apoptosis using the ouabain-sensitive uptake of Rb assay. Figure 8 shows typical X-ray spectra and quantitative data for Rb Lα peaks from fractions of total and ouabain-insensitive Rb uptake in control and STS-treated cells. After 3 and 5 h of exposure to STS, we noted significant decreases ($P < 0.01$ and $P < 0.001$, respectively) in total Rb uptake fraction in comparison with untreated control cells. The difference between total and ouabain-insensitive fractions of Rb uptake resulted in a decrease in ouabain-sensitive Rb uptake (net activity), indicating a decrease in functional activity of the Na^+/K^+ ATPase pump in STS-induced apoptotic cells. Decreased activity of the Na^+/K^+ ATPase pump coincided with caspase-3 activation, PARP cleavage, changes in chromatin, and DNA fragmentation. We also noted a significant decrease in ouabain-insensitive Rb uptake after 5 h in comparison with untreated control cells and cells treated with STS for 3 h.

Figure 7. Electron probe X-ray microanalysis of rubidium (Rb) uptake in U937 cells after staurosporine (STS) treatment. The Rb-uptake assays were performed by adding 5 mM RbCl to non-treated or treated U937 cells with 1 μM STS. At different times, cells were cryoprocessed as explained in the legend to Figure 4. Semiquantitative data (peak/background ratio) are shown for Rb uptake in untreated (*filled circles*) and STS-treated cells (*open circles*). Data are given as the mean ± standard error of the mean of 3 independent experiments. Significant differences between groups are indicated by an asterisk (*, $P < 0.01$; **, $P < 0.001$).

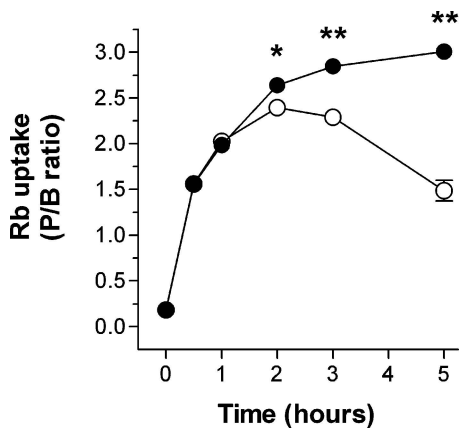

Discussion

In this report we examine the temporal relationship between changes in total elemental composition and activation of caspase-3, cell shrinkage, DNA fragmentation and nuclear breakage during apoptosis induced by STS, an inducer of the apoptotic-mitochondrial pathway. Measuring elemental concentrations at the single cell level with EPXMA, we established two distinct phases in the progression of apoptosis, each characterized by a distinctive pattern of changes in intracellular elements, particularly in K, Cl and Na. Previously, Okada and Maeno[1] identified two distinct stages in cell volume changes during mitochondrion- or death receptor-mediated apoptosis: an early stage starting before the formation of the apoptosome and activation of effector caspases, and a later stage concurrent with the appearance of the nuclear features of apoptosis. Here we demonstrate that the first phase, which lasts until 2 h after exposure to STS, was characterized by a decrease in intracellular concentration (mmol/kg dry weight) of K and Cl. These elemental alterations precede the activation of caspase-3, which is detected in significant amounts 2 h after STS treatment is begun. The second phase, which commences with the cleavage of caspase-3 and PARP, was characterized by an increase in intracellular Na and a decrease in K. During this phase intracellular Cl content increases in comparison to the first phase. At the end of this phase there is a significant decrease in intracellular S, which leads in turn to an increase in P/S ratio. These changes in elemental content coincide with DNA fragmentation and nuclear breakage.

Early studies with EPXMA in UV-induced apoptotic cells reported alterations in Na, Cl and K.[36] However, the previous study did not provide a detailed time-course of elemental changes or information about the relationship between these changes and the typical early molecular features of apoptosis. Another study with EPXMA reported similar elemental alterations in Na, Cl and K in association with DNA fragmentation detected by terminal transferase-mediated DNA nick-end labelling (TUNEL), a late molecular hallmark of apoptosis.[37] These microanalytical results have recently been confirmed in etoposide-induced apoptosis in prostate cancer cell lines.[38] However, in the LNCaP androgen-sensitive cell line, Cl content increased after androgen withdrawal and etoposide treatment.[39] This would, in principle, contradict the notion that AVD is associated with the activation of cation and anion pathways similar to those triggered during RVD which cause an efflux of K^+

Figure 8. Na^+/K^+-ATPase function in untreated, control and staurosporine (STS)-induced apoptotic cell death. The functional expression of the Na^+/K^+-ATPase pump was assessed as ouabain-sensitive Rb uptake measured by electron probe X-ray microanalysis. Fifteen minutes prior to the end of the assay, control and STS-treated U937 cells were exposed to 1 mM ouabain for 15 min. After incubation, cells used for total and ouabain-insensitive transport were loaded with 5 mM RbCl for 10 min and cryoprocessed as described in the legend to Figure 4. (A.) X-ray spectra from fractions of cells used for total and ouabain-insensitive Rb uptake under both experimental conditions. (B.) Semiquantitative data (peak/background ratio) for Rb Lα peaks in control and STS-treated cells. Total Rb-uptake (*open bars*), ouabain-insensitive Rb-uptake (*shadow bars*), and ouabain-sensitive Rb-uptake (*filled bars*). Note the significant decrease in ouabain-sensitive Rb uptake (net activity) after 3 and 5 h of STS exposure. Data are given as the mean ± standard error of the mean of 3 independent experiments. Significant differences between groups are indicated by different superscripts (a, b, and c) according to the Kruskall-Wallis test and Dunn's multiple comparisons test.

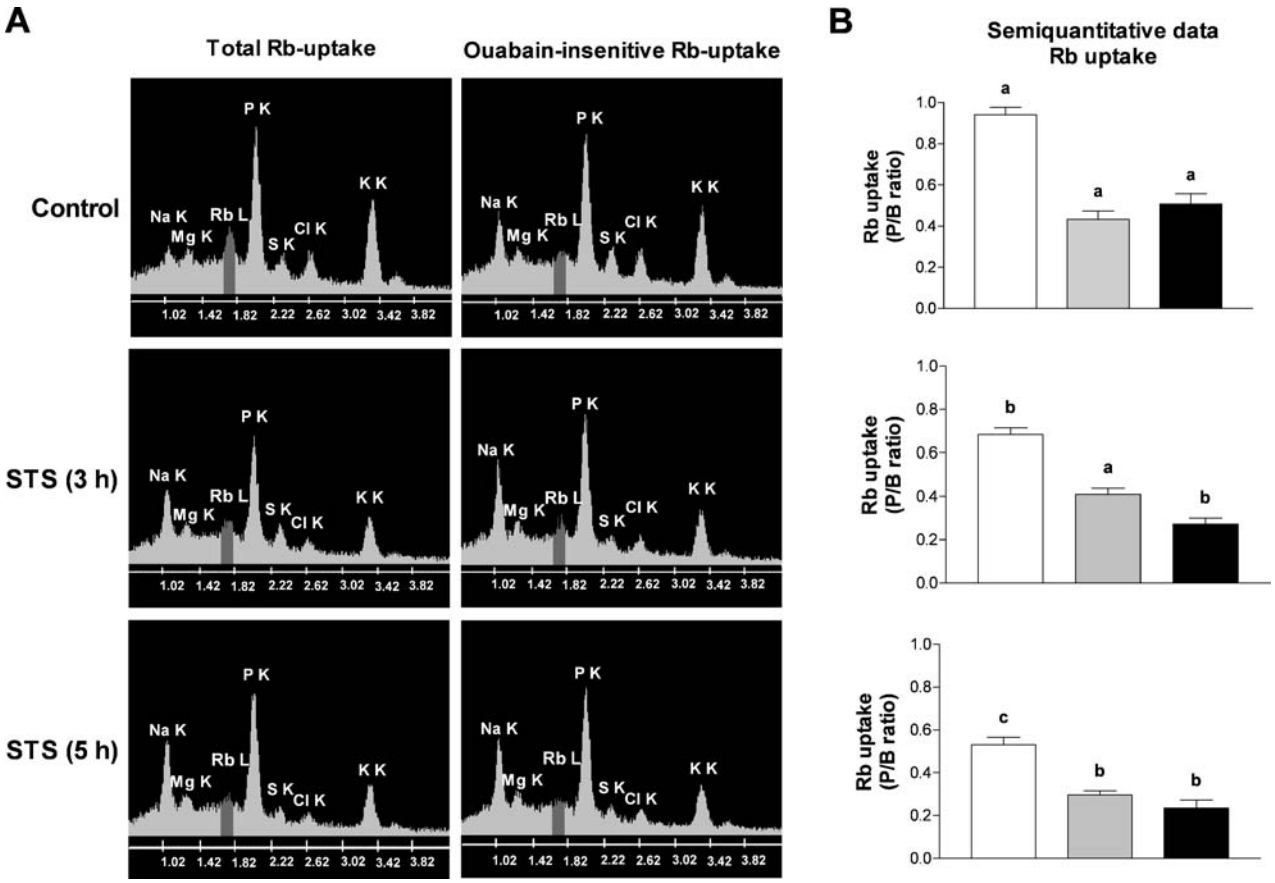

and Cl^- via volume-regulated ion channels.[13,16,40] Our findings in human U937 cells suggest that the changes these authors found in elemental concentrations in apoptotic cells were recorded in later phases of apoptosis, before loss of integrity of the plasma membrane.

Electron probe X-ray microanalysis makes it possible to relate alterations in elemental homeostasis, especially K, Cl, and Na, with different features of cell death characteristic of apoptosis. In addition, we were able to document correlations between changes in different elements. Previous studies with multiparametric flow cytometry have reported correlations only between the hallmarks of apoptosis and alterations in K^+ concentrations. Early studies in apoptotic thymocytes reported that the loss of cytosolic K^+ occurs after dissipation of the mitochondrial membrane potential and mitochondrial swelling, but before cell shrinkage and before the plasma membrane becomes permeable.[5,41] However, studies in Jurkat T cells treated with anti-Fas showed that K^+ efflux was concomitant with the loss of cell volume, loss of mitochondrial membrane potential and externalization of phosphatidylserine, and was restricted to shrunken apoptotic cells that showed degradation of DNA and activation of executioner caspases.[2,42] Similar results were obtained when K^+ efflux was monitored with the $^{86}Rb^+$ assay.[14] Here we demonstrated that the decrease in intracellular K content occurs early, concomitantly with cell shrinkage, but before caspase-3 activation, PARP cleavage, chromatin condensation or DNA fragmentation. The reason for these discrepant findings is unknown,

although they may be related with the specific apoptotic pathway that is activated under each experimental condition.

This early decrease in K content was concomitant with a decrease in intracellular Cl content during the first phase of apoptosis. This means that the alteration in Cl also coincided with the significant loss of cell volume occurring prior to the typical molecular and morphological features of STS-induced apoptosis. Our quantitative data for both elements are consistent with studies in several types of cell (Jurkat T, HeLa, U937, and PC-12) exposed to STS, which showed that AVD was sensitive to pharmacological blockers of K^+ and Cl^- channels involved in cell volume regulation.[13,16,40] However, a recent study based on electrophysiological methods indicated that STS-induced apoptosis in ECV304 cells generated a rapid increase in plasma membrane Cl^- channel activity, which was not accompanied by an increase in K^+ conductance.[43] However, because of methodological difficulties with electrophysiological experiments designed to measure K^+ currents, the authors could not rule out the possibility of involvement of K^+ channels during AVD.

The low Cl content during the first phase of apoptosis is probably related with the efflux of Cl^- as a result of the electrochemical gradient created by the efflux of K^+. It has also been suggested that membrane hyperpolarization caused by the increase in K^+ currents might activate Cl^- efflux and reduce intracellular Cl^- concentration.[44] Both situations would lead to the accumulation of KCl outside the cell, which in turn would favor the extrusion of water from the cell in an attempt to restore a normal osmotic gradient.[45] However, little is known concerning the type of Cl^- channel involved in the activation of Cl^- currents during AVD. It has been suggested that activation of volume-sensitive outwardly rectifying (VSOR) or VSOR-like Cl^- channels may be involved.[1,13,40,46] Activation of the VSOR Cl^- channel was recently found to be mediated by reactive oxygen species during normotonic cell shrinkage in HeLa cells exposed to STS.[47]

The simultaneous decrease in K and Cl content was seen only during the first phase of STS-induced apoptosis. Beginning with caspase-3 activation, a time-dependent increase in intracellular Cl content was evident with respect to the early phase. To our knowledge this is the first report of this association. This time-course of the increase in Cl was similar to that of chromatin condensation and DNA fragmentation. However, this finding is difficult to interpret because some studies propose that the importance of Cl^- efflux for the control of DNA fragmentation factor 40 (DFF40) occurs somewhere downstream of caspase-3 and DFF40/DFF45 proteolysis.[46,48] Also, a reduction of Cl^- efflux by using NaCl to raise extracellular osmolarity or by Cl^- channel blockers prevents oligonucleosomal DNA cleavage.[23] However, our work does not exclude the possibility that the decrease in Cl content observed during the first phase of apoptosis is responsible for controlling the activity of DFF40.

The increase in Cl was also associated with an increase in intracellular Na content which could be considered a sign that the cell is unable to sustain the intracellular Cl^- deficit after depolarization of the plasma membrane. The demonstration with EPXMA that the increase in Cl was associated with inversion of the intracellular K and Na concentrations as a consequence of inhibition of the Na^+/K^+-ATPase pump during the second stage of STS-induced apoptosis supports this possibility. Depolarization of the plasma membrane with ouabain, an inhibitor of Na^+/K^+-ATPase pump, induces passive Cl^- uptake via Cl^- channels.[49] Moreover, during the execution phase of apoptosis, the significant loss of intracellular K is the result of dysfunction of Na^+/K^+-ATPase in combination with possibly enhanced K^+ efflux via K^+ permeable channels.[50]

Studies with flow cytometry to evaluate changes in Na^+ homeostasis during apoptosis have yielded contradictory results. A preliminary study with a Na^+-sensitive indicator showed an increase in Na^+ content in mouse L cells after treatment with etoposide.[51] In contrast, later studies with multiparametric flow cytometry reported a loss of intracellular K^+ and Na^+.[4,17] Recently, an increase in intracellular Na^+ has been described upon anti-Fas induced apoptosis in Jurkat T-cells.[31] The increase occurs early, correlates with plasma membrane depolarization, and occurs before the decrease in K^+ and loss of cell volume. Studies with EPXMA also reported an increase in Na content during UV- or oxLDL-induced apoptosis in U937 cells and macrophages, respectively.[36,37] Here, we found that the increase in Na coincides with caspase-3 activation, chromatin condensation and DNA fragmentation. In addition, the increase in Na parallels the decrease in intracellular K and the increase in Cl. These findings suggest that the increase in Na occurs later during the second phase of STS-induced apoptosis.

The reasons for the increase in Na are not well understood, although a role for the inhibition of Na^+/K^+-ATPase, the primary role of which is maintain high intracellular K^+ and low intracellular Na^+, has been suggested. This hypothesis is supported by evidence that inhibition of Na^+/K^+-ATPase with ouabain during apoptosis enhanced cell death in different model systems[31,52–54] and by the inhibition of Na^+/K^+-ATPase during apoptosis induced by anti-Fas in Jurkat T-cells[31,52] and C_2-ceramide or serum deprivation in cortical neurons.[54–56] Here we report inhibition of the functional expression of Na^+/K^+-ATPase; accordingly, the distinctive changes in elemental composition during the second phase of apoptosis, *i.e.*, the inversion of intracellular K and Na content, may be attributable in part to inhibition of the Na^+, K^+-pump. In addition, the fact that element changes were not associated with an increase in the release of

LDH rules out the possibility that these changes were the result of mechanical damage to the plasma membrane. Taken together, these findings suggest that impairment of the Na^+, K^+-pump is a generalized response to mitochondrion- or death receptor-mediated apoptosis. However, further research will be needed to test this hypothesis.

The cause of Na^+/K^+-ATPase inhibition remains controversial. Some authors have proposed specific cleavage of the regulatory β-subunit of the Na^+ pump.[31,53] Another line of research has been suggested that Na^+/K^+-ATPase β-subunit degradation and the associated plasma membrane depolarization are coupled to mitochondrial membrane depolarization.[57] Others have suggested that failure of the pump results from concurrent ATP depletion and oxidant stress.[56] Our findings do not rule out any of these possibilities, although it is interesting to note that in STS-treated U937 cells with the molecular and nuclear features of apoptosis, the mitochondria appear swollen (unpublished observations). Recently, we demonstrated that the distinctive ion profile of the execution phase of apoptosis coincides with dissipation of the mitochondrial membrane potential.[58]

Conclusion

This study documents the precise sequence of changes in total elemental composition during staurosporine-induced apoptosis, revealing two distinctive stages in the changes in K, Cl and Na content. The elemental profile in the early stage (low K and Cl) was related with cell shrinkage, whereas the changes in the late stage (low K, high Cl and Na) were related with molecular and morphological hallmarks of apoptosis. Additionally, our work shows that inversion of the intracellular proportions of K and Na during the second stage was related, in part, with impairment of the Na^+/K^+-ATPase pump. Future research will focus on the definition of the sequence of total electrolyte changes during different signal pathways that regulate apoptosis in order to determine whether the alterations in elemental concentrations documented here represent a universal response.

Acknowledgments

The authors thank Ms Maria A. Robles for her expert technical assistance with immunocytochemistry and K. Shashok for improving the use of English in the manuscript. This work was supported by grants from the Fondo de Investigaciones Sanitarias (FIS), Instituto de Salud Carlos III (Contract grant numbers FIS 01/0937 and PI021622).

References

1. Okada Y, Maeno E, Shimizu T, Dezaki K, Wang J, Morishima S. Receptor-mediated control of regulatory volume decrease (RVD) and apoptotic volume decrease (AVD). *J Physiol* 2001; **532**: 3–16.
2. Bortner CD, Cidlowski JA. Caspase independent/dependent regulation of K^+, cell shrinkage, and mitochondrial membrane potential during lymphocyte apoptosis. *J Biol Chem* 1999; **274**: 21953–21962.
3. Hughes FM, Bortner CD, Purdy GD, Cidlowski JA. Intracellular K^+ suppresses the activation of apoptosis in lymphocytes. *J Biol Chem* 1997; **272**: 30567–30576.
4. McCarthy JV, Cotter TG. Cell shrinkage and apoptosis: a role for potassium and sodium efflux. *Cell Death Differ* 1997; **4**: 756–770.
5. Dallaporta B, Hirsch T, Susin SA, *et al.* Potassium leakage during the apoptotic degradation phase. *J Immunol* 1998; **160**: 5605–5615.
6. Yu SP, Yeh CH, Sensi SL, *et al.* Mediation of neuronal apoptosis by enhancement of outward potassium current. *Science* 1997; **278**: 114–117.
7. Yu SP, Yeh CH, Gottron F, Wang X, Grabb MC, Choi DW. Role of the outward delayed rectifier K^+ current in ceramide-induced caspase activation and apoptosis in cultured neurons. *J Neurochem* 1999; **73**: 933–941.
8. Wang L, Xu D, Dai W, Lu L. An ultraviolet-activated K^+ channel mediates apoptosis of myeloblastic leukemia cells. *J Biol Chem* 1999; **274**: 3678–3685.
9. Nietsch HH, Roe MW, Fiekers JF, Moore AL, Lidofsky SD. Activation of potassium and chloride channels by tumor necrosis factor α. Role in liver cell death. *J Biol Chem* 2000; **275**: 20556–20561.
10. Krick S, Platoshyn O, Sweeney M, Kim H, Yuan JXJ. Activation of K^+ channels induces apoptosis in vascular smooth muscle cells. *Am J Physiol Cell Physiol* 2001; **280**: C970–C979.
11. Krick S, Platoshyn O, McDaniel SS, Rubin LJ, Yuan JXJ. Augmented K currents and mitochondrial membrane depolarization in pulmonary artery myocyte apoptosis. *Am J Physiol Lung Cell Mol Physiol* 2001; **281**: L887–L894.
12. Trimarchi JR, Liu L, Smith PJS, Keefe DL. Apoptosis recruits two-pore domain potassium channels used for homeostatic volume regulation. *Am J Physiol Cell Physiol* 2002; **282**: C588–C594.
13. Maeno E, Ishizaki Y, Kanaseki T, Hazama A, Okada Y. Normotonic cell shrinkage because of disordered volume regulation is an early prerequisite to apoptosis. *Proc Natl Acad Sci USA* 2000; **97**: 9487–9492.
14. Thompson GJ, Langlais C, Cain K, Conley EC, Cohen GM. Elevated extracellular $[K^+]$ inhibits death-receptor- and chemical-mediated apoptosis prior to caspase activation and cytochrome c release. *Biochem J* 2001; **357**: 37–145.
15. Brevnova EE, Platoshyn O, Zhang S, Yuan JXJ. Overexpression of human *KCNA5* increases and enhances apoptosis. *Am J Physiol Cell Physiol* 2004; **287**: C715–C722.
16. Szabó I, Lepple-Wienhues A, Kaba KN, Zoratti M, Gulbins E, Lang F. Tyrosine kinase-dependent activation of a chloride channel in CD95-induced apoptosis in T lymphocytes. *Proc. Natl. Acad. Sci. USA* 1998; **95**: 6169–6174.
17. Bortner CD, Hughes FM, Cidlowski JA. A primary role for K^+ and Na^+ efflux in the activation of apoptosis. *J Biol Chem* 1997; **272**: 32436–32442.
18. Bortner CD, Cidlowski JA. Uncoupling cell shrinkage from apoptosis reveals that Na^+ influx is required for volume loss

during programmed cell death. *J Biol Chem* 2003; **278**: 39176–39184.
19. Thornberry NA, Lazebnik Y. Caspases: Enemies within. *Science* 1998; **281**: 1312–1316.
20. Zimmerman KC, Bonzon C, Green DR. The machinery of programmed cell death. *Pharmacol Ther* 2001; **92**: 57–70.
21. Cain K, Langlais C, Sun XM, Brown DG, Cohen GM. Physiological concentration of K^+ inhibit cytochrome c-dependent formation of the apoptosome. *J Biol Chem* 2001; **276**: 41985–41990.
22. King KL, Jewell CM, Bortner CD, Cidlowski JA. 28S ribosome degradation in lymphoid cell apoptosis: Evidence for caspase and Bcl-2-dependent and -independent pathways. *Cell Death Differ* 2000; **7**: 994–101.
23. Rassola A, Far DF, Hofman P, Rossi B. Lack of internucleosomal DNA fragmentation is related to Cl^- efflux impairment in hematopoietic cell apoptosis. *FASEB J* 1999; **13**: 1711–1723.
24. Courageot MP, Lépine S, Hours M, Giraud F, Sulpice JC. Involvements of sodium in early phosphatidylserine exposure and phospholipid scrambling by P2X7 purinoreceptor in thymocytes. *J Biol Chem* 2004; **279**: 21815–21823.
25. Andersson C, Roomans GM. Determination of chloride efflux by X-ray microanalysis versus MQAE-fluorescence. *Microsc Res Tech* 2002; **59**: 531–535.
26. Haddad P, Beck JS, Boyer JL, Graf J. Role of chloride ions in liver cell regulation. *Am J Physiol Gastrointest Liver Physiol* 1991; **261**: G340–G348.
27. Fernández-Segura E, Cañizares FJ, Cubero MA, Warley A, Campos A. A procedure to prepare cultured cells in suspension for electron probe X-ray microanalysis: Application to scanning and transmission electron microscopy. *J Microsc* 1999; **196**: 19–25.
28. Warley A, Skepper JN. Long freeze-drying times are not necessary during the preparation of thin sections for X-ray microanalysis. *J Microsc* 2000; **198**: 116–23.
29. Roomans GM. Quantitative electron probe X-ray microanalysis of biological specimens. *J Electron Microsc Tech* 1988; **9**: 19–44.
30. Warley A. X-ray microanalysis for biologists. London: Portland Press 1997.
31. Bortner CD, Gómez-Angelats M, Cidlowski JA. Plasma membrane depolarization without repolarization is an early molecular event in anti-Fas-induced apoptosis. *J Biol Chem* 2001; **276**: 4304–4314.
32. Bertrand R, Solary E, O'Connor P, Kohn KW, Pommier Y. Induction of common pathway of apoptosis by staurosporine. *Exp Cell Res* 1994, **211**: 314–321.
33. Mills JC, Stone NL, Erhardt J, Pittman RN. Apoptotic membrane blebbing is regulated by myosin light chain phosphorylation. *J Cell Biol* 1998, **140**: 627–636.
34. Abraham EH, Breslow JL, Epstein J, Chang-Sing P, Lechene C. Preparation of individual human diploid fibroblasts and study of ion transport. *Am J Physiol* 1985; **248**: C154–C164.
35. Zierold K. Effects of cadmium on electrolyte ions in cultured rat hepatocytes studied by X-ray microanalysis of cryosections. *Toxicol Appl Pharmacol* 1997; **144**: 70–76.
36. Fernández-Segura E, Cañizares FJ, Cubero MA, Warley A, Campos A. Changes in elemental content during apoptotic cell death studied by electron probe X-ray microanalysis. *Exp Cell Res* 1999; **253**: 454–462.
37. Skepper JN, Karydis I, Garnett MR, *et al.* Changes in elemental concentrations are associated with early stages of apoptosis in human monocyte-macrophages exposed to oxidized low-density lipoprotein: An X-ray microanalytical study. *J Pathol* 1999; **188**: 100–106.
38. Salido M, Vilches J, Lopez A, Roomans GM. Neuropeptides bombesin and calcitonin inhibit apoptosis-related elemental changes in prostate carcinoma cell lines. *Cancer* 2002; **94**: 368–377.
39. Salido M, Vilches J, Roomans GM. Changes in elemental concentration in LNCaP cells are associated with a protective effect of neuropeptides on etoposide-induced apoptosis. *Cell Biol Int* 2004; **28**: 397–402.
40. Okada Y, Maeno E, Shimizu T, Manabe K, Mori S, Nabekura T. Dual roles of plasmalemmal chloride channels in induction of cell death. *Pflügers Arch* 2004; **448**: 287–295.
41. Dallaporta B, Marchetti P, de Pablo MA, *et al.* Plasma membrana potential in thymocyte apoptosis. *J Immunol* 1999; **162**: 6534–6542.
42. Vu CCQ, Bortner CD, Cidlowski JA. Differential involvement of initiator caspases in apoptotic volume decrease and potassium efflux during Fas- and UV-induced cell death. *J Biol Chem* 2001; **276**: 37602–37611.
43. Porcelli AM, Ghelli A, Zanna C, Valente P, Ferroni S, Rugolo M. Apoptosis induced by staurosporine in ECV304 cells require cell shrinkage and upregulation of Cl^- conductance. *Cell Death Differ* 2004; **11**: 655–662.
44. Platoshyn O, Zhang S, McDaniel SS, Yuan JXJ. Cytochrome c activates K^+ channels before inducing apoptosis. *Am J Physiol Cell Physiol* 2002; **283:** C1298–C1305.
45. Remillard CV, Yuan XJJ. Activation of K^+ channels: An essential pathway in programmed cell death. *Am J Physiol Lung Cel Mol Physiol* 2004; **286:** L49–L67.
46. Dupéré-Minier G, Hamelin C, Desharnais P, Bernier J. Apoptotic volume decrease, pH acidification and chloride channel activation during apoptosis requires CD45 expression in HPB-ALL T cells. *Apoptosis* 2004; **9**: 543–551.
47. Shimizu T, Numata T, Okada Y. A role of reactive oxygen in apoptotic activation of volume-sensitive Cl(-) channel. *Proc Natl Acad Sci USA* 2004; **101**: 6770–6773.
48. Widlak P, Garrard WT. Discovery, regulation, and action of the major apoptotic nucleases DFF40/CAD and endonuclease G. *J Cell Biochem* 2005; **94**: 1078–1087.
49. Krep H, Lefurgey A, Graves SW, Hockett D, Ingram P, Hollenberg NK. Elemental composition of Na pump inhibited rabbit aorta VSM cells by electron probe X-ray microanalysis. *Am J Physiol* 1996; **271**: H514–H520.
50. Yu SP, Regulation and critical role of potassium homeostasis in apoptosis. *Prog Neurobiol* 2003; **70**: 363–386.
51. Barbiero G, Duranti F, Bonelli G, Amenta J, Baccino FM. Intracellular ionic variations in apoptotic death of L cells by inhibitors of cell cycle progression. *Exp Cell Res* 1995; **217**: 410–418.
52. Nobel CSI, Aronson J, van den Dobbelsteen DJ, Slater AFG. Inhibition of Na^+/K^+-ATPase may be one mechanism contributing to potassium efflux and cell shrinkage in CD95-induced apoptosis. *Apoptosis* 2000; **5**: 153–163.
53. Mann CL, Bortner CD, Jewell CM, Cidlowski JA. Glucocorticoid-induced plasma membrane depolarization during tymocytes apoptosis: Association with cell shrinkage and degradation of the Na^+/K^+-adenosine triphosphatase. *Endocrinology* 2001; **142**: 5059–5068.
54. Xiao AY, Wang XQ, Yang A, Yu SP. Slight impairment of Na^+,K^+-ATPase synergistically aggravates ceramide- and β-amyloid-induced apoptosis in cortical neurons. *Brain Res* 2002; **955**: 253–259.
55. Xiao AY, Wei L, Xia S, Rothman S, Yu SP. Ionic mechanism of ouabain-induced concurrent apoptosis and necrosis in individual cultured cortical neurons. *J Neurochem* 2002; **22**: 1350–1362.

56. Wang XQ, Xiao AY, Sheline C, *et al.* Apoptotic insults impair Na^+,K^+-ATPase activity as a mechanism of neuronal death mediated by concurrent ATP deficiency and oxidant stress. *J Cell Sci* 2003; **116**: 2099–2110.
57. Düssmann H, Rehm M, Kögel D, Prehn JHM. Outer mitochondrial membrane permeabilization during apoptosis triggers caspase-independent mitochondrial and caspase-dependent membrane potential depolarization: a single-cell analysis. *J Cell Sci* 2003; **116**: 525–536.
58. Arrebola F, Zabiti S, Cañizares FJ, Cubero MA, Crespo PV, Fernández-Segura E. Changes in intracellular sodium, chlorine, and potassium concentrations in staurosporine-induced apoptosis. *J Cell Physiol* 2004; **204**: 500–507.